

Loop closure detection using local 3D deep descriptors

Youjie Zhou¹, Yiming Wang², Fabio Poiesi³, Qi Qin¹ and Yi Wan¹

Abstract—We present a simple yet effective method to address loop closure detection in simultaneous localisation and mapping using local 3D deep descriptors (L3Ds). L3Ds are emerging compact representations of patches extracted from point clouds that are learned from data using a deep learning algorithm. We propose a novel overlap measure for loop detection by computing the metric error between points that correspond to mutually-nearest-neighbour descriptors after registering the loop candidate point cloud by its estimated relative pose. This novel approach enables us to accurately detect loops and estimate six degrees-of-freedom poses in the case of small overlaps. We compare our L3D-based loop closure approach with recent approaches on LiDAR data and achieve state-of-the-art loop closure detection accuracy. Additionally, we embed our loop closure approach in RESLAM, a recent edge-based SLAM system, and perform the evaluation on real-world RGBD-TUM and synthetic ICL datasets. Our approach enables RESLAM to achieve a better localisation accuracy compared to its original loop closure strategy.

Index Terms—Loop Closure Detection; 3D Local Descriptors; Simultaneous Localization and Mapping

I. INTRODUCTION

Loop closure aims to recognise already visited places in order to mitigate tracking drifts in simultaneous localisation and mapping (SLAM) [1]. Correctly handling loop closures can improve localisation accuracy of an autonomous robot [2]. Typically, loop closure is a self-contained module involving *detection*, *pose estimation* and *verification*, which is executed in parallel with other processes during SLAM [3].

A loop closure is detected when enough 2D or 3D overlap is measured between the viewpoint of a current keyframe and of a previous one [2]. While in 2D one can use visual representations extracted from keyframe images based on, e.g., bags of binary words [3], [4] or fern-based bag of words [2], [5], to detect loops, in 3D one can match geometric or semantic representations between pairs of point clouds across time [6]–[10]. Representations can be built by aggregating local geometric information [6] or by globally encoding the whole point cloud into a signature [7], [8], [10], [11]. Local geometries can be encoded as bag-of-words, extracted from randomly sampled 3D points and matched through similarity

measures (e.g. L2 norm) [6]. Global methods often exploit the 2D projections of point clouds, and quantify the overlap of two point clouds using either handcrafted measures [7], [8], or via a deep neural network [10].

Pose estimation aims to determine a six degrees-of-freedom (6DoF) transformation between viewpoints. One way to determine this transformation is to compute point-to-point correspondences of 2D features tracked over time [3], [12]. However, features may be wrongly associated or lost during tracking, due to sudden camera motion or viewpoint variations. Alternatively, the 6DoF transformation can be determined by processing point clouds, i.e. through 3D point-to-point (or to-plane) associations [13], local descriptors [6] or direct pose regression [10]. Iterative Closest Points (ICP) [13] is the gold standard for point-to-point registration, however ICP is prone to failure when point clouds are significantly mis-aligned. In the case of significant mis-alignments, local 3D descriptors can be used to register a pair of points through RANSAC [6], [14], [15]. Recent deep-learning-based 3D descriptors [14]–[16] have outperformed the handcrafted descriptors [17], achieving state-of-the-art point cloud registration accuracy with a promising generalisation capability. Poses can also be directly estimated through regression with a Siamese deep network that operates on the whole point cloud, however it requires a certain overlap between pairs to function properly: to estimate the 1DoF transformation between a pair, the minimum overlap should be about 30% [10], while for the 6DoF transformation, the overlap should be greater than 70% [18].

In this letter, we present a novel approach to detect loop closures while performing 6DoF pose estimation with local 3D deep descriptors (L3Ds). Our approach is based on an overlap measure that we compute as the Ratio Of Nearest points in both the descriptor and metric space, namely *RON*. Specifically, we quantify the overlap between a point cloud pair by computing the metric error of the registered points that are mutually nearest neighbours in the descriptor space. The relative 6DoF transformation between point clouds is estimated using RANSAC with L3Ds. L3Ds are inferred by a deep network from randomly sampled points within each point cloud. Then, *RON* is computed as the ratio of corresponding points that have a small metric error.

Our L3D-based loop detection approach outperforms the state-of-the-art methods *OverlapNet* [10] and *LiDAR Iris* [8], which are validated using the LiDAR point clouds from the KITTI odometry dataset [19]¹. We use the same evaluation strategy presented in *OverlapNet* [10]. Moreover, we show

^{*}This work has been submitted to the IEEE for possible publication. Copyright may be transferred without notice, after which this version may no longer be accessible.

^{*}This work was supported by the China government (2019JZZY010112) and (2020JMRH0202)

¹Youjie Zhou, Qi Qin and Yi Wan are with the School of Mechanical Engineering, Shandong University, China 202020511@mail.sdu.edu.cn

²Yiming Wang is with Deep Visual Learning (DVL) Unit, Fondazione Bruno Kessler, Italy, ywang@fbk.eu

³Fabio Poiesi is the corresponding author and he is with Technologies of Vision (TeV) Unit, Fondazione Bruno Kessler, Italy, poiesi@fbk.eu

¹We will release the code upon acceptance.

the efficacy of our approach to RGBD SLAM systems by embedding it into RESLAM [2], a recent RGBD edge-based SLAM approach. We evaluate the absolute trajectory error [20] on the real-world TUM-RGBD [20] and synthetic ICL [21] datasets. Our approach enables RESLAM to detect loops more frequently and to estimate 6DoF transformations more accurately than those estimated with the RESLAM’s original loop closure method.

II. RELATED WORK

We review recent loop closure detection methods that are designed for 3D data, e.g. point clouds. Readers are referred to [1] for a more thorough review on general loop closure methods. Existing research on 3D-based loop detection can be categorised into three groups [22]: feature-based [7], [8], [11], [23]–[25], segmentation-based [26], [27], and learning-based methods [9], [10], [28], [29].

Earlier methods are mostly focused on hand-crafted rotation-invariant 3D descriptors, often using histograms to encode point features, such as FPFH [30] or global shape features [8], [31]. One way to build global features is via Normal Distribution Transform (NDT) by representing the point cloud as a set of normal distributions [23]. 3D scans can be divided into overlapping cells, where for each cell the mean vector and covariance matrix are computed, and instances of certain classes of NDT in range intervals define the feature histogram. Rotation invariance is achieved by aligning scans with respect to dominant surface orientations. Differently, M2DP [7] forms the global feature by projecting the point cloud to multiple 2D planes and generates a density signature where the left and right singular vectors of these signatures are used as global descriptor. Often, global descriptors encode only the geometric properties of the point cloud, Intensity Scan Context [11] instead encodes both the geometry and intensity of LIDAR scans. Karl *et al.* [25] define 41 features of the full scan to create decision stumps, and learn a binary classifier with Adaboost for loop detection, followed by RANSAC-based registration using point feature FPFH [24]. A recent global descriptor, known as LiDAR Iris [8], has been proposed for fast and accurate loop closure detection, under the inspiration of the human’s iris signature for identification. Each LiDAR scan is firstly converted to a binary signature image after several LoG-Gabor filtering and thresholding operations. The Hamming distance of a pair is then used for detecting the loop. The above-mentioned hand-crafted features are rotation-invariant and somewhat robust in handling noise, yet still limited in capturing the complex scene structure, making them prone to erroneous loop detections.

Segmentation-based methods encode the point cloud into a set of distinctive features which reduce the likelihood of obtaining false matches. SegMatch [26] does not assume perfect semantic segmentation, and uses two hand-crafted features, i.e. eigenvalue-based and shape histograms, to describe each segment and performs the matching with random forest with RANSAC-based geometric verification. Seed [27] proposes handcrafted features that encode the topological information

of segmented objects to reduce the noise and resolution effect. Both SegMatch and Seed uses the cluster-all method to segment the point cloud and requires the ground plane removal prior to the segmentation.

Learning-based methods are also proposed to address loop closure detection. LocNet [28] proposes a handcrafted rotation-invariant representation of point cloud in a image-like format, and applies a Siamese network to learn a global feature of scan maps for place matching and loop closure detection. With the advances in 3D deep learning, Zaganidis *at al.* [32] use semantics from PointNet++ [33] together with the NDT-based histogram descriptors for loop closure detection. GOSMatch [29] further propose a semantic-level global descriptor that is a histogram-based graph descriptor that encodes relations of objects segmented by RangeNet++ [34]. Instead of performing frame-by-frame loop detection, SegMap [9] segments the scene incrementally as the robot navigates and gives these segments to a deep network as input to generate a signature per segment. Loop detection is then performed based on segments. Recently, OverlapNet [10] presented a Siamese deep neural network to exploit different types of information of LiDAR scans, including depth, normals, intensity or remission values, to predict the overlap and relative yaw angle between pairs of 3D scans.

In general, most of the above-mentioned methods only estimate the relative yaw angle among two LiDAR scans, as the public LiDAR datasets, such as KITTI [19] or nuScenes [35] are acquired by autonomous vehicles where scans are often assumed to be co-planar. Moreover, the learning based methods are mostly trained and tested on data belonging the same domain, e.g. LiDAR data in outdoors, which cannot generalise well to other domains without retraining or finetuning, such as sparser point clouds reconstructed with vision-based SLAM systems [36]. Differently, our approach exploits advanced deep local 3D descriptors that are trained with point clouds extracted from RGBD sensors, estimates the 6DoF transformation between a pair of point clouds, and measures the overlap, serving for the loop closure detection task with little domain gap.

III. L3D-BASED LOOP CLOSURE

A typical SLAM system involves three modules running in parallel that are tracking, local mapping and global mapping [2], [3]. Tracking computes the relative camera motion between consecutive frames. The most informative frames are stored as keyframes. Local mapping processes every new keyframe to incrementally reconstruct the map of the environment and optimises the reconstruction using a time-shifting window. Global mapping performs loop closure and relocalisation using pose graph optimisation. Loop closure aims to address the problems of finding keyframes that can potentially form trajectory loops, estimating the poses between candidate keyframe pairs and verifying that the candidate loop closure is correctly estimated. It is important to detect and solve loops correctly as they would otherwise increase the trajectory error.

Our proposed L3D-based approach identifies the candidate loop frames by measuring the overlap amongst local 3D descriptors that are extracted between keyframe pairs, and then confirms the occurrence of a loop through pose estimation and RON computation. In the following sections, we describe the 3D descriptor extraction in Sec. III-A, and the algorithms for loop detection and confirmation in Sec. III-B.

A. 3D descriptor extraction

Given a 3D point and a set of its neighbouring points, namely a patch, a local 3D descriptor is a compact numerical representation of these points [14]–[16], [37].

Let $\mathcal{P}_t = \{\mathbf{p}_t\} \subset \mathbb{R}^3$ be the point cloud of the current keyframe at frame t that is defined as an unordered set of 3D points, and $\Pi_t = [\mathcal{P}_{t-1}, \dots, \mathcal{P}_0]$ be an ordered collection of point clouds stored up to frame $t - 1$, with $t > 0$. The size of this collection and the number of points of each point cloud may vary over time and across scenes. At each t , we randomly choose a set of $n_t = n \cdot |\mathcal{P}_t|$ points as centres for our 3D descriptors, where $n \in \mathbb{R}_{(0,1]}$ and $|\cdot|$ is the cardinality of a set. The subsampled point cloud is defined as $\tilde{\mathcal{P}}_t \subset \mathcal{P}_t$ where $|\tilde{\mathcal{P}}_t| = n_t$. Let $\mathcal{D}_t = \{\mathbf{d}_t\} \subset \mathbb{R}^d$ be the set of d -dimensional descriptors where $|\mathcal{D}_t| = |\tilde{\mathcal{P}}_t|$.

Given a point in $\tilde{\mathcal{P}}_t$, we can extract a patch composed of neighbouring points within a spherical region of radius ρ , and use a deep neural network to encode this patch into a compact descriptor. Let $\mathcal{X}_t = \{\mathbf{x}_t\} \subset \mathcal{P}_t$ be the patch extracted from \mathcal{P}_t and $\mathbf{d}_t = \Phi_\Theta(\mathcal{X}_t)$, where Φ_Θ is the deep neural network with parameters Θ that encodes \mathcal{X}_t into the descriptor \mathbf{d}_t , such that $\|\mathbf{d}_t\| = 1$. We experimentally select the best-performing deep neural network for the descriptor encoding, more details can be found in Sec. IV-C.

B. Loop detection and verification

When a loop occurs, it is highly likely that a portion of the current keyframe’s point cloud overlaps with a portion of another point cloud in previous keyframes. Except for some occluded parts, there should exist corresponding surfaces between these overlapping point cloud portions, thus corresponding descriptors. The higher this overlap is, the higher the likelihood of detecting a loop. We detect candidate loops through the estimation of the overlap between point cloud pairs in the descriptor space, and confirm the occurrence of a loop by computing (i) the transformation to register a candidate point cloud pair and (ii) the novel overlap measure *RON* that measures the ratio of nearest points in both the descriptor and metric space.

Specifically, we determine the overlap region between the two point clouds $\tilde{\mathcal{P}}_t$ and $\tilde{\mathcal{P}}_{t'}$, where $t' < t$, by selecting points whose descriptors, \mathcal{D}_t and $\mathcal{D}_{t'}$, are mutually nearest neighbours (MNN). The computation of MNN descriptors is efficient and does not require the estimation of the transformation matrix between two viewpoints. Let $\mathcal{C}_{t,t'}$ be the set of corresponding points defined as

$$\begin{aligned} \mathcal{C}_{t,t'} &= \{\{\mathbf{p}_t \in \tilde{\mathcal{P}}_t, \mathbf{p}_{t'} \in \tilde{\mathcal{P}}_{t'}\} : \mathbf{d}_t = \text{NN}(\mathbf{d}_{t'}, \mathcal{D}_t) \wedge \mathbf{d}_{t'} \\ &= \text{NN}(\mathbf{d}_t, \mathcal{D}_{t'})\}, \end{aligned} \quad (1)$$

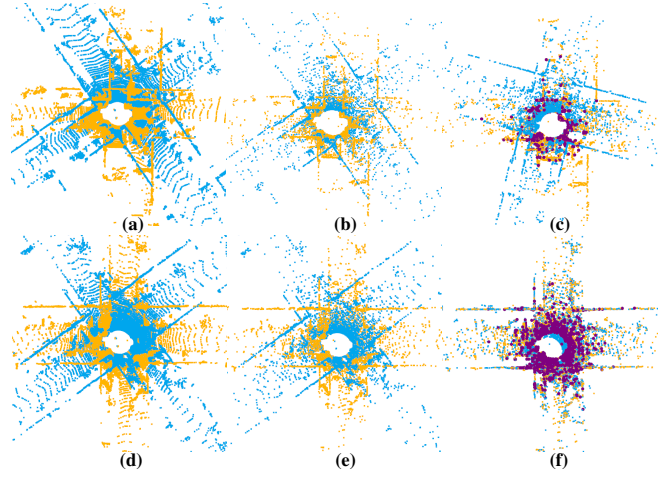


Fig. 1. Two examples of point cloud pairs of LiDAR scans where the pair in first row does not form a loop, and the pair in the second row does. (a, d) are the pair of original LiDAR scans indicated by different colors. (b, e) are the subset of points that correspond to descriptor-wise MNNs. (c, f) are the points that correspond to the descriptor-wise MNNs after the RANSAC registration. Points that are close to each other in the metric space are highlighted in purple.

where $\text{NN}(\cdot)$ is the nearest neighbour search based on the L2 norm. We infer the MNN overlap between the two point clouds as

$$o_{t,t'} = \frac{|\mathcal{C}_{t,t'}|}{\min\{|\mathcal{D}_t|, |\mathcal{D}_{t'}|\}}, \quad (2)$$

where $o_{t,t'} \in \mathbb{R}_{[0,1]}$. If the overlap $o_{t,t'}$ is greater than a threshold τ_o , then we deem these keyframes to form a candidate loop.

Points with the corresponding descriptors being mutually neighbours does not necessarily guarantee the points in the metric space are also close to each other. To verifying the loop, we further register the candidate pairs by estimating the relative 6DoF transformation and estimate RON for the loop confirmation.

Different methods can be used to register two point clouds [38], [39]. Without loss of generality, we use RANSAC [38] as we found that it performs well in practice in terms of computational efficiency and robustness to noise. Let $\mathbf{T}_{t,t'} \in \mathbb{R}^{4 \times 4}$ be the transformation estimated with RANSAC between $\tilde{\mathcal{P}}_t$ and $\tilde{\mathcal{P}}_{t'}$ using \mathcal{D}_t and $\mathcal{D}_{t'}$, respectively.

Finally, with the registered point clouds, we compute RON as the ratio of MNN points in the descriptor space that are close in the metric space, i.e. whose distance in the metric space is below a certain error. Let RON be $\mathcal{F}_{t,t'}$ that is defined as

$$\mathcal{F}_{t,t'} = \frac{1}{|\mathcal{C}_{t,t'}|} \sum_{\{\mathbf{p}_t, \mathbf{p}_{t'}\} \in \mathcal{C}_{t,t'}} \|\mathbf{p}_t - \mathbf{T}_{t,t'} \circ \mathbf{p}_{t'}\|_2 < \tau_e, \quad (3)$$

where $\|\cdot\|_2$ is the L2 norm, \circ is the operator that applies $\mathbf{T}_{t,t'}$ to a 3D point and τ_e is the maximum error between two corresponding points that takes into account the reconstruction noise. If $\mathcal{F}_{t,t'}$ is greater than a threshold $\tau_{\mathcal{F}}$, then we confirm the occurrence of a loop.

Fig. 1 illustrates the effects of RON in the case of a non-loop and of a loop. The top row shows a pair of LiDAR

Algorithm 1: Open3D-style pseudocode for L3D-based loop detection.

```
# P_ta: point cloud of keyframe at ta
# P_tb: point cloud of keyframe at tb < ta
# D_ta: descriptors of the points in P_ta
# D_tb: descriptors of the points in P_tb
# phi_theta: descriptor encoder algorithm
# nn(x, y): nearest-neighbour (NN) search in the set x
# using queries y
# T: transformation to register P_ta on P_tb
# tau_e: max distance between corresponding points

def mnn(D_ta, D_tb):
    # compute the indices of D_tb that are the NN of the
    # queries D_ta
    inds_b = nn(D_tb, D_ta)
    # compute the indices of D_ta that are the NN of the
    # queries D_tb
    inds_a = nn(D_ta, D_tb)
    # compute boolean list w.r.t. inds_a
    # true entries correspond to mutual NN elements
    mnn_bools = list(range(len(D_ta)) == inds_a[inds_b])
    return mnn_bools, inds_b

def loop_detection(P_ta, P_tb, D_ta, D_tb, T, tau_e):
    # compute mutual nearest neighbours
    mnn_bools, inds_b = mnn(D_ta, D_tb)
    # compute overlap
    o = mnn_bools.sum() / min([len(D_ta), len(D_tb)])
    # apply transformation
    P_ta.transform(T)
    # compute L2 norm between mutual NN points
    dists = norm(P_ta.points - P_tb.points[inds_b])
    # compute ration of nearest points (RON)
    f = (dists[mnn_bools] < tau_e).sum() / mnn_bools.sum()
    return o, f
```

scans that are captured in a similar neighbourhood (Fig. 1 (a)), resulting in a large amount of points that are MNN in the descriptor space (Fig. 1 (b)). These MNN points can be further filtered by registering the two point clouds and by estimating RON (Fig. 1 (c)). The bottom row shows a pair of LiDAR scans that are captured in the same location, i.e., a loop (Fig. 1 (d)), leading to a large amount of points that are MNN in the descriptor space (Fig. 1 (e)). Amongst the MNN points, a large number of them are also close to each other in the metric space after registration (Fig. 1 (f)), i.e. resulting in a correct loop detection as the RON value is high.

The transformation $T_{t,t'}$ can be fed to the module in charge of solving the pose graph problem to optimise the camera poses in any SLAM system. The pseudocode for our loop verification approach is shown in Algorithm 1.

IV. EXPERIMENTS

We evaluate our approach with two experiments using LiDAR SLAM and visual RGBD SLAM to show its general applicability. Our approach outperforms alternative methods in various scenarios. Firstly, we compare our approach against recent LiDAR-based loop closure approaches, namely *OverlapNet* [10] and *LiDAR Iris* [8], using the LiDAR dataset KITTI odometry [40]. Secondly, we embed our loop closure method in a recent visual SLAM system, and test it on a real RGBD dataset, TUM-RGBD [20], and on a synthetic RGBD dataset, ICL [21]. We choose the edge-based visual SLAM method, namely *RESLAM* [2], as the point clouds produced by the mapping are different from those of KITTI.

Throughout the experiments, we use DIP descriptors as the L3D [15], as it achieves the best performance in terms

of point cloud registration across domains (see Sec. IV-C for more details), thus no need for retraining. DIP processes the input point clouds in two steps. First, it estimates a local reference frame from the point clouds of the patch to canonicalise the patch in order to make the descriptor rotation-invariant. Second, a deep neural network encodes the canonicalised patch into a compact descriptor. More details of the DIP descriptor are referred to [15]. We use the same descriptor parameters as presented in [15], except for the radius of the patch. We use 2.5m as the patch radius for KITTI, and 0.2m for TUM RGBD and ICL.

A. Loop closure detection for LiDAR SLAM

We compare our approach against two recent LiDAR-based methods [8], [10] for loop closure detection.

OverlapNet [10] estimates the overlap with a deep neural network with the inputs extracted from the LiDAR scans containing both the geometric and semantic information. *OverlapNet* defines the overlap between a scan pair as the ratio of the projected range pixels within 1m over all valid range pixels, where the candidate scan pairs are projected into range images with a common coordinate system. For fair evaluation, we reproduce the results using the provided model with inputs reflecting only geometrical information, i.e. depths, normals and intensities.

LiDAR Iris [8] uses a global descriptor for LiDAR scans. Each scan is converted into a binary signature image using a series of LoG-Gabor filtering and thresholding operations. *LiDAR Iris* defines the overlap as the Hamming distance of a pair of the binary signature images. We reproduce the results using the provided code to generate the signature images and compute the Hamming distance.

Within this comparative evaluation, we also assess three variants of our L3D-based loop detection approach, namely *L3D-based Overlap* that quantifies the overlap following the ground-truth overlap computation as in *OverlapNet* [10], *L3D-based MNN* that quantifies the overlap only as the ratio of MNN, i.e. via Eq. 2, and *L3D-based RON* that quantifies the overlap as the proposed RON, i.e., via Eq. 3.

Evaluation protocol. We follow the evaluation protocol proposed in *OverlapNet* [10], where a set of criteria are used for the detection of loop given a sequence. We use Sequence 00 of KITTI odometry for the test. As the vehicle moves, each current scan serves as a query. For each query, the latest 100 scans are excluded from the candidates to avoid detecting a loop closure in the most recent scans. Like most of the SLAM systems, the candidate loop scans are constrained within the 3σ area around the current pose estimate. We use the same series of pose uncertainty as in [10] for the σ estimation. Amongst the valid candidate loop scans, only those with the highest estimated overlap are considered throughout this evaluation. A true positive is determined if the ground-truth overlap is larger than 30%.

Discussion. Fig. 2 illustrate the Precision-Recall (PR) curves. Note that no training on KITTI was performed with our L3D-based methods, while *OverlapNet* is trained with the KITTI odometry using Sequences 03-10, and *LiDAR Iris*

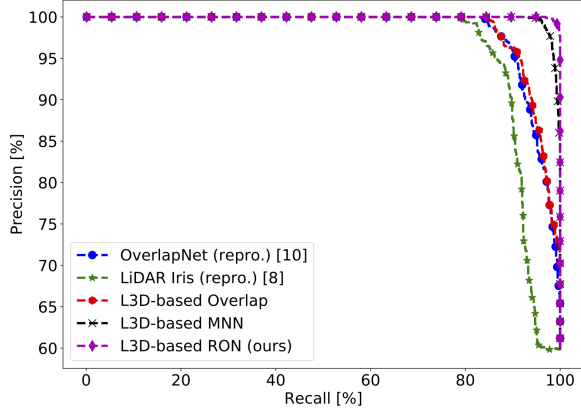


Fig. 2. The precision and recall curve of loop closure detection that compares variants of our approach based on local 3D deep descriptors (L3D) and the state-of-the-art methods, i.e. OverlapNet [10] and LiDAR Iris [8].

is particularly designed for matching LiDAR scans. Generalisation to unseen scenarios (sensors, environments) is a highly desired property for the deployment of robots in real-world applications. *L3D-based Overlap* produces a similar PR curve to OverlapNet, indicating that the relative transformations computed by RANSAC using the local 3D descriptors can achieve comparable performances to global loop closure detection methods. Note that here we estimate the 6DoF transformation, while OverlapNet estimates the 1DoF transformation. As shown by *L3D-based MNN* curve, when we use the ratio of MNN in the descriptor space as the overlap measure, the PR curve can further improve. *L3D-based RON* achieves the best PR curve, which justifies that the proposed overlap measure is the most effective and reliable one. To achieve a high RON value, it requires the points to be not only MNN in the descriptors space but also geometrically close to each other after the estimated transformation. descriptor space (Fig. 1 (b)). These MNN points can be further filtered by registering the two point clouds and by estimating RON (Fig. 1 (c)). The bottom row shows a pair of LiDAR scans that are captured in the same location, i.e., a

B. Loop Closure for Visual SLAM

For the evaluation of visual RGBD SLAM, we use nine sequences from TUM-RGBD and seven sequences from ICL. TUM-RGBD contains real scenes recorded with a Kinect at 30Hz and its ground truth is captured using a motion capture system working at 100Hz. ICL contains photo-realistic scenes rendered with a simulated Kinect at 20-30Hz, featuring real-world trajectories captured using a motion capture system working at 100Hz.

We use the recent RESLAM [2] to serve as the overall SLAM system where we embed our proposed approach. Original RESLAM performs the selection of candidate keyframe pairs based on the similarity between the current and the previous keyframes using 2D visual cues, i.e. Fern. If none of the previous keyframes yields a sufficient similarity

with the current one, the loop closure is terminated, and a global and compact representation of the new keyframe is added to a database. Otherwise a geometric-based assessment is further carried out using PGO.

We use the original parameters of RESLAM and set $n = 0.4$, $\tau_o = 0.13$, $\tau_e = 10cm$ and $\tau_{\mathcal{F}} = 0.2$ (see notations Sec. III-B). We set the max number of RANSAC iterations to 500K and the termination policy to 1K iterations for an average inlier error of 3cm. We report the results of RESLAM from their paper [2] and also include our reproduced results as the authors of [2] stated that different hardware may provide different results.

We use RESLAM [repro.1] and RESLAM [repro.2] to refer to the results reproduced by us using two configurations of RESLAM: the former uses the original parameters, the latter has parameters set to detect loop closures more frequently. The evaluation of the latter was performed to show the behaviour of RESLAM with a number of detected loops comparable to those of our approach. We also evaluate an ablated version of our approach, i.e. only the module to estimate the transformation matrix between the keyframe and loop frame based on DIP, i.e. we turned off Alg. 1. This ablation experiment is designed to show the benefit of using DIP descriptors for pose estimation after the loop closures detected with RESLAM’s visual cues.

Evaluation metrics. We evaluate our approach by comparing the absolute errors between the estimated and the ground-truth trajectories, noted as ATE, by computing the root mean squared error (RMSE) of the translational component [20]. Given that the rigid-body transformation \mathbf{S} corresponding to the least-squares solution that maps the estimated pose of the camera \mathbf{C}_t onto its ground-truth pose \mathbf{G}_t at frame t , ATE can be computed as $\mathcal{E}_t = \mathbf{G}_t^{-1}\mathbf{S}\mathbf{C}_t$. The RMSE is computed over all the frames of each sequence as

$$RMSE_{\mathcal{E}} = \sqrt{\frac{1}{n} \sum_{t=1}^{t_{\text{end}}} \|\text{trans}(\mathcal{E}_t)\|^2}, \quad (4)$$

where t_{end} is the number of frames of a given sequence.

Discussion. Tab. I and Tab. II report the results of our approach where we can observe that for the majority of the sequences we can improve the localisation accuracy of RESLAM. We run our algorithm multiple times on a subset of sequences of Tab. I and Tab. II to assess the numerical stability of the results and we obtained stable results across different runs. We can observe a reduced ATE in almost all sequences (Except for *fr1/xyz*, when we use DIP descriptors only to estimate the transformation between the keyframes forming loops (i.e. no Alg. 1)). When we employ our loop detection approach, we can see an overall reduction of the ATE. The main reason of this is due to the detection of a larger number of loops and thus a more frequent triggering of pose graph optimisation that tends to reduce the trajectory error.

We show in Fig. 3 some qualitative results on RGBD-TUM and ICL. These sequences include a variety of trajectory patterns, i.e. from the handheld camera of *fr1/room* to the

TABLE I

COMPARISON OF THE ROOT MEAN SQUARED ERROR COMPUTED OVER ALL FRAMES OF THE TRANSLATIONAL COMPONENTS OF THE ABSOLUTE TRAJECTORY ERROR IN [CM] ON THE RGBD-TUM DATASET. ITALIC FONT IS FOR RESULTS FROM [2], BOLD FONT HIGHLIGHTS THE BEST RESULT. RESLAM [REPRO.1] IS OUR REPRODUCED VERSION OF RESLAM WITH ORIGINAL SETUP. RESLAM [REPRO.2] IS OUR REPRODUCED VERSION OF RESLAM WHERE WE ALLOW FOR MORE FREQUENT LOOP DETECTIONS. IN PARENTHESIS (·) WE REPORT THE NUMBER OF DETECTED LOOPS.

seq.	RESLAM [2]	RESLAM [repro.1]	RESLAM [repro.2]	OURS [no Alg.1]	OURS [full]
fr1/xyz	<i>1.1</i>	2.3 (27)	2.3 (27)	2.3 (27)	1.8 (27)
fr1/room	-	8.6 (3)	9.6 (11)	8.5 (3)	6.4 (14)
fr1/plant	-	8.6 (1)	6.7 (6)	7.3 (3)	7.0 (5)
fr1/desk	-	2.7 (5)	2.7 (7)	2.7 (5)	2.7 (7)
fr1/rpy	-	2.9 (19)	2.6 (25)	2.9 (19)	2.6 (25)
fr1/desk2	<i>4.8</i>	6.3 (7)	5.8 (15)	3.8 (8)	3.6 (17)
fr2/desk	<i>1.9</i>	2.2 (24)	128.8 (25)	2.2 (24)	2.2 (38)
fr2/xyz	<i>0.5</i>	0.4 (14)	0.4 (15)	0.5 (16)	0.5 (16)
fr3/office	3.5	3.8 (8)	24.0 (15)	3.8 (10)	3.4 (15)
average		4.2	20.3	3.8	3.4

TABLE II

COMPARISON OF THE ROOT MEAN SQUARED ERROR COMPUTED OVER ALL FRAMES OF THE TRANSLATIONAL COMPONENTS OF THE ABSOLUTE TRAJECTORY ERROR IN [CM] ON THE ICL DATASET. BOLD FONT HIGHLIGHTS THE BEST RESULT. RESLAM [REPRO.1] IS OUR REPRODUCED VERSION OF RESLAM WITH ORIGINAL SETUP. RESLAM [REPRO.2] IS OUR REPRODUCED VERSION OF RESLAM WHERE WE ALLOW FOR MORE FREQUENT LOOP DETECTIONS. IN PARENTHESIS (·) WE REPORT THE NUMBER OF DETECTED LOOPS.

seq.	RESLAM [repro.1]	RESLAM [repro.2]	OURS [no Alg.1]	OURS [full]
deer/walk	10.1 (15)	30.7 (33)	8.6 (26)	6.0 (48)
deer/Mfast	1.0 (89)	1.0 (92)	1.0 (82)	1.0 (106)
deer/Mslow	1.7 (110)	3.6 (126)	1.7 (112)	1.6 (139)
deer/run	5.4 (4)	19.1 (9)	3.5 (7)	2.6 (16)
diamond/walk	7.2 (9)	19.3 (22)	7.4 (11)	3.8 (46)
diamond/Mfast	1.0 (87)	0.9 (92)	1.0 (89)	0.9 (105)
diamond/run	14.4 (2)	10.8 (7)	8.6 (6)	6.0 (10)
average	5.8	12.1	4.5	3.1

micro aerial vehicle mounted camera of *diamond/Mfast*. We can visually appreciate how the trajectory estimated using our proposed L3D-based loop closure approach is much closer to the ground-truth one. Some part of these trajectories are indicated with a purple bounding box to highlight the improvement.

Fig. 4 shows some registration results on the keyframes corresponding to detected loops when the 6DoF transformation is estimated using the RESLAM’s loop closure approach and ours. We can observe that the registration that is obtained with RESLAM provides a systematic misalignment. We noticed this also on other sequences. At times, the transformation estimated with RESLAM is incorrect, see c) and d), while our loop closure approach can often register the keyframes correctly.

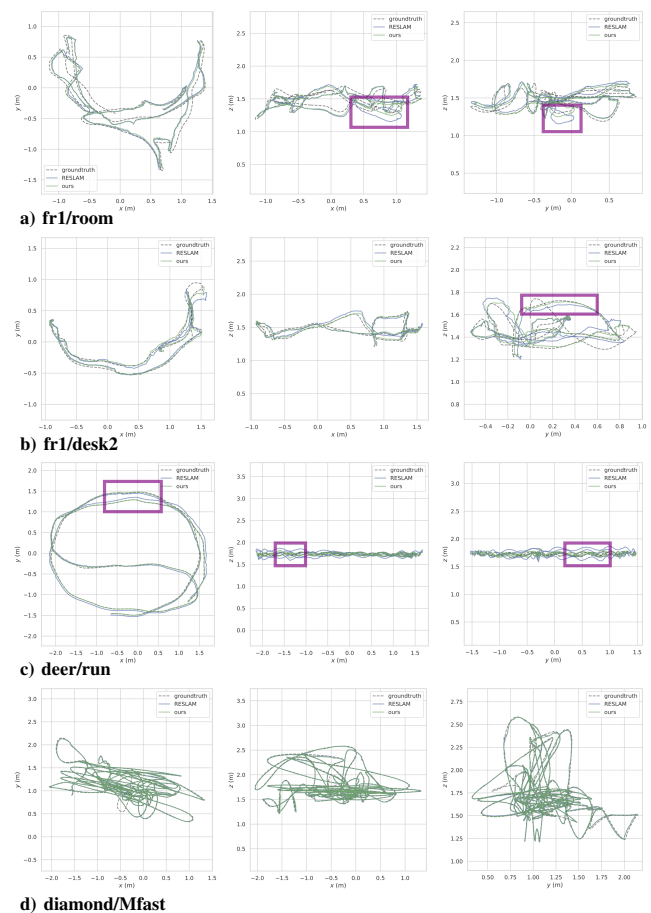


Fig. 3. Trajectories obtained with the original RESLAM’s loop closure approach and with our approach on (a,b) TUM-RGBD and (c,d) ICL sequences, projected on the xy , xz and yz planes. Purple bounding boxes show examples where our approach improves localisation.

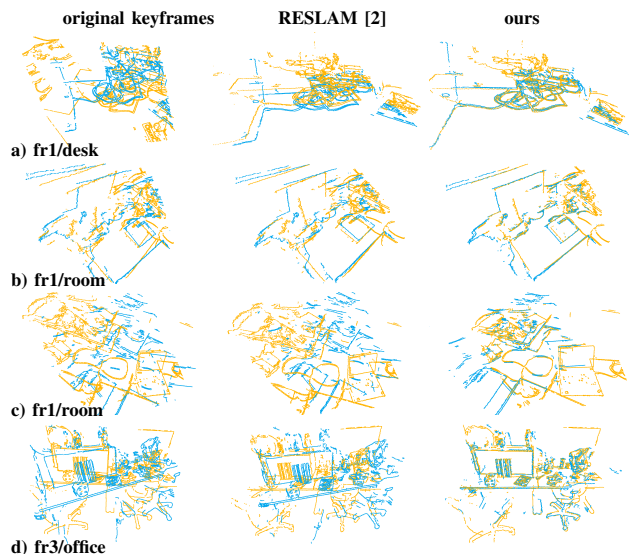


Fig. 4. Edge point cloud registration results using the original RESLAM’s loop closure approach and ours.

Lastly, Fig. 5 and Fig. 6 shows qualitative localisation and mapping results using our loop closure approach. From these examples we can observe the full structure of the

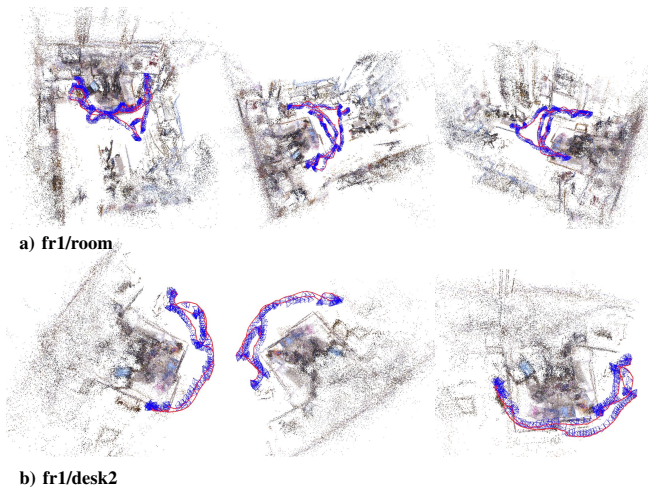


Fig. 5. Examples of localisation and mapping results using our loop closure approach on TUM-RGBD dataset. The trajectory is shown in red and the camera poses in blue.



Fig. 6. Examples of localisation and mapping results using our loop closure approach on ICL dataset. The trajectory is shown in red and the camera poses in blue.

environment in the form of coloured point cloud.

C. Analysis of 3D descriptors

We provide a quantitative analysis of traditional and recent 3D deep descriptors using the TUM-RGBD dataset. This experiment motivates the choice of DIP descriptor as opposed to other descriptors in the literature. As the performance measure, we adopt the registration recall [15], [37], which measures the ratio of point cloud pairs whose average distance error between the corresponding points after being registered by the estimated transformation is below 0.2m.

We use the edge-based point clouds extracted from four sequences of TUM-RGBD using RESLAM. For each sequence we randomly select 1000 point cloud pairs with at least 30% overlap. We compare four descriptors, one handcrafted approach, namely FPFH [17], and three deep learning based approaches: one global approach, namely FCGF [16], and two local approaches, namely SpinNet [14] and DIP [15]. For FPFH we used its Open3D implementation, whereas for the others, we used the code and models provided by the authors. For all the deep learning based descriptors, we use

TABLE III

REGISTRATION RECALL AND COMPUTATION TIME PER DESCRIPTOR IN [MS] COMPUTED ON FOUR SEQUENCES OF RGBD TUM DATASET.

	fr1/desk	fr1/desk2	fr1/plant	fr1/room	mean	[ms]
FPFH [17]	0.35	0.39	0.34	0.41	0.37	0.02
FCGF [16]	0.58	0.46	0.41	0.52	0.50	0.03
SpinNet [14]	0.71	0.75	0.85	0.75	0.76	10.18
DIP [15]	0.73	0.76	0.85	0.77	0.78	3.79

their models trained on 3DMatch [41].

Tab. III shows the results of this experiment. FPFH and FCGF are the fastest descriptors to compute, however at a large cost of the registration error. DIP achieves the best registration recall with a better compromise between the computation efficiency and the registration performance compared to SpinNet.

V. CONCLUSION

We presented a novel approach to address loop closures using deep learning-based 3D local descriptors [15]. Our approach detects loop candidates using the ratio of mutually nearest-neighbour descriptors and confirms their quality by computing the novel measure, namely RON, the ratio of metrically near points amongst points that are mutually nearest neighbours in the descriptor space. We evaluated the approach for both LiDAR-based and visual SLAM system loop closure detection. Results showed that our approach can outperform the state-of-the-art LiDAR-based loop closure detection methods, and further improves the localisation accuracy of the visual SLAM system as well. Future research directions include fusing 2D visual cue extracted from images with 3D local descriptors to handle scenes lacking geometric structures, and focus on the optimisation of descriptor computation.

REFERENCES

- [1] S. Arshad and G.-W. Kim, "Role of deep learning in loop closure detection for visual and LIDAR SLAM: A survey," *Sensors*, vol. 21, no. 4, pp. 12–43, Feb 2021.
- [2] F. Schenk and F. Fraundorfer, "RESLAM: A real-time robust edge-based SLAM system," in *Proc. of IEEE International Conference on Robotics and Automation*, Montreal, CA, May 2019.
- [3] R. Mur-Artal and J. Tardos, "ORB-SLAM2: An open-source slam system for monocular, stereo, and RGB-D cameras," *IEEE Trans. on Robotics*, vol. 33, no. 5, p. 1255–1262, Oct 2017.
- [4] D. Galvez-Lopez and J. Tardos, "Bags of binary words for fast place recognition in image sequences," *IEEE Trans. on Robotics*, vol. 28, no. 5, pp. 1188–1197, Oct 2012.
- [5] B. Glocker, J. Shotton, A. Criminisi, , and S. Izadi, "Real-time rgb-d camera relocalization via randomized ferns for keyframe encoding," *IEEE Trans. on Visualization and Computer Graphics*, vol. 21, no. 5, p. 571–583, Sep 2015.
- [6] "Place recognition in 3D scans using a combination of bag of words and point feature based relative pose estimation," in *Proc. of IEEE International Conference on Intelligent Robots and Systems*, San Francisco, US, Sep 2011.
- [7] L. He, X. Wang, and H. Zhang, "M2DP: A novel 3D point cloud descriptor and its application in loop closure detection," in *Proc. of IEEE International Conference on Intelligent Robots and Systems*, Daejeon, KR, Oct 2016.
- [8] Y. Wang, Z. Sun, C.-Z. Xu, S. Sarma, J. Yang, and H. Kong, "LiDAR Iris for Loop-Closure Detection," in *Proc. of IEEE IROS*, Virtual, Jan 2021.

- [9] R. Dube, A. Cramariuc, D. Dugas, J. Nieto, R. Siegwart, and C. Cadena, "SegMap: Segment-based mapping and localization using data-driven descriptors," *International Journal of Robotics Research*, vol. 39, no. 2-3, pp. 339–355, Mar 2020.
- [10] X. Chen, T. Labe, A. Milioto, T. Rohling, O. Vysotska, A. Haag, J. Behley, and C. Stachniss, "OverlapNet: Loop closing for LiDAR-based SLAM," in *Proc. of RSS*, Virtual, Jul 2020.
- [11] H. Wang, C. Wang, and L. Xie, "Intensity scan context: Coding intensity and geometry relations for loop closure detection," in *Proc. of IEEE International Conference on Robotics and Automation*, Virtual, Aug 2020.
- [12] B. Horn, "Closed-form solution of absolute orientation using unit quaternions," *Journal of the Optical Society of America A*, vol. 4, no. 4, p. 629–642, 1987.
- [13] P. Besl and N. McKay, "A method for registration of 3D shapes," *IEEE Trans. on Pattern Analysis and Machine Intelligence*, vol. 14, no. 2, pp. 239–256, Feb 1992.
- [14] S. Ao, Q. Hu, B. Yang, A. Markham, and Y. Guo, "SpinNet: Learning a General Surface Descriptor for 3D Point Cloud Registration," in *Proc. of IEEE CVPR*, Virtual, Jun 2021.
- [15] F. Poiesi and D. Boscaini, "Distinctive 3D local deep descriptors," in *Proc. of IEEE International Conference on Pattern Recognition*, Virtual, Jan 2021.
- [16] C. Choy, J. Park, and V. Koltun, "Fully Convolutional Geometric Features," in *Proc. of IEEE International Conference on Computer Vision*, Seoul, KR, Oct 2019.
- [17] R. Rusu, N. Blodow, and M. Beetz, "Fast Point Feature Histograms (FPFH) for 3D registration," in *Proc. of IEEE International Conference on Robotics and Automation*, Kobe, JP, May 2009.
- [18] X. Li, J. Pontes, and S. Lucey, "PointNetLK Revisited," in *Proc. of IEEE CVPR*, Virtual, Jun 2021.
- [19] A. Geiger, P. Lenz, C. Stiller, and R. Urtasun, "Vision meets robotics: The kitti dataset," *The International Journal of Robotics Research*, vol. 32, no. 11, pp. 1231–1237, 2013.
- [20] J. Sturm, N. Engelhard, F. Endres, W. Burgard, and D. Cremers, "A benchmark for the evaluation of RGBD SLAM systems," in *Proc. of IEEE Intelligent Robots and Systems*, Vilamoura, PT, Oct 2012.
- [21] S. Saeedi, E. Carvalho, W. Li, D. Tzoumanikas, S. Leutenegger, P. Kelly, and A. Davison, "Characterizing visual localization and mapping datasets," in *Proc. of IEEE ICRA*, Montreal, CA, May 2019.
- [22] Z. Wang, Y. Shen, B. Cai, and M. Saleem, "A brief review on loop closure detection with 3D point cloud," in *Proc. of IEEE Real-time Computing and Robotics*, Irkutsk, RU, Aug 2019.
- [23] M. Magnusson, H. Andreasson, A. Nuchter, and A. Lilienthal, "Automatic appearance-based loop detection from three-dimensional laser data using the normal distributions transform," *Journal of Field Robotics*, vol. 26, no. 11-12, pp. 892–914, Nov 2009.
- [24] T.-L. Habich, M. Stuede, M. Labbe, and S. Spindeldreier, "Have i been here before? learning to close the loop with LiDAR data in graph-based SLAM," *arXiv:2103.06713*, May 2021.
- [25] K. Granstrom and T. Schon, "Learning to close the loop from 3D point clouds," in *Proc. of IEEE International Conference on Intelligent Robots and Systems*, Taipei, TW, Oct 2010.
- [26] R. Dube, D. Dugas, E. Stumm, J. Nieto, R. Siegwart, and C. Cadena, "SegMatch: Segment based place recognition in 3D point clouds," in *Proc. of IEEE International Conference on Robotics and Automation*, Singapore, May 2017.
- [27] Y. Fan, Y. He, and U.-X. Tan, "Seed: A segmentation-based egocentric 3D point cloud descriptor for loop closure detection," in *Proc. of IEEE International Conference on Intelligent Robots and Systems*, Las Vegas, US, Oct 2020.
- [28] H. Yin, L. Tang, X. Ding, Y. Wang, and R. Xiong, "LocNet: Global Localization in 3D Point Clouds for Mobile Vehicles," in *Proc. of IEEE Intelligent Vehicles Symposium*, Suzhou, CN, Jun 2018.
- [29] Y. Zhu, Y. Ma, L. Chen, C. Liu, M. Ye, and L. Li, "GOSMatch: Graph-of-Semantics Matching for Detecting Loop Closures in 3D LiDAR data," in *Proc. of IEEE Intelligent Robots and Systems*, Las Vegas, US, Oct 2020.
- [30] R. Rusu, N. Blodow, and M. Beetz, "Fast point feature histograms (FPFH) for 3D registration," in *Proc. of IEEE International Conference on Robotics and Automation*, Kobe, JP, May 2009.
- [31] T. Rohling, J. Mack, and D. Schulz, "A fast histogram-based similarity measure for detecting loop closures in 3-d lidar data," in *Proc. of IEEE Intelligent Robots and Systems*, Hamburg, GE, Sep 2015.
- [32] A. Zaganidis, A. Zernitev, T. Duckett, and G. Cielniak, "Semantically assisted loop closure in slam using ndt histograms," in *Proc. of IEEE Intelligent Robots and Systems*, Macao, CN, Nov 2019.
- [33] C. Qi, L. Yi, H. Su, and L. Guibas, "Pointnet++: deep hierarchical feature learning on point sets in a metric space," in *Proc. of Neural Information Processing Systems*, Long Beach, US, Dec 2017.
- [34] A. Milioto, I. Vizzo, J. Behley, and C. Stachniss, "Rangenet++: Fast and accurate lidar semantic segmentation," in *Proc. of IEEE Intelligent Robots and Systems*, Macao, CN, Nov 2019.
- [35] H. Caesar, V. Bankiti, A. H. Lang, S. Vora, V. E. Liong, Q. Xu, A. Krishnan, Y. Pan, G. Baldan, and O. Beijbom, "nusScenes: A multimodal dataset for autonomous driving," in *Proceedings of the IEEE/CVF conference on computer vision and pattern recognition*, 2020, pp. 11 621–11 631.
- [36] S. Zhang, L. Zheng, and W. Tao, "Survey and evaluation of rgb-d slam," *IEEE Access*, vol. 9, pp. 21 367–21 387, 2021.
- [37] Z. Gojcic, C. Zhou, J. Wegner, and W. Andreas, "The perfect match: 3D point cloud matching with smoothed densities," Long Beach, US, Jun 2019.
- [38] M. Fischler and R. Bolles, "Random sample consensus: A paradigm for model fitting with applications to image analysis and automated cartography," *Commun. ACM*, vol. 24, no. 6, pp. 341–406, Jun 1981.
- [39] J. P. Q.-Y. Zhou and V. Koltun, "Fast global registration," in *Proc. of ECCV*, Amsterdam, NL, Oct 2016.
- [40] A. Geiger, P. Lenz, and R. Urtasun, "A fast histogram-based similarity measure for detecting loop closures in 3-d lidar data," in *Proc. of IEEE CVPR*, Providence, US, Jun 2012.
- [41] A. Zeng, S. Song, M. Niessner, M. Fisher, J. Xiao, and T. Funkhouser, "3DMatch: Learning the matching of local 3D geometry in range scans," in *Proc. of IEEE Computer Vision and Pattern Recognition*, Hawaii, US, Jul 2017.